Multifunctional Quantum Dot Nanoparticles for Effective Differentiation and Long-Term Tracking of Human Mesenchymal Stem Cells In Vitro and In Vivo

*Jinming Li, Wayne Yukwai Lee, Tianyi Wu, Jianbin Xu, Kunyu Zhang, Gang Li, Jiang Xia, and Liming Bian**

Human mesenchymal stem cells (hMSCs) hold great potential for regenerative medicine. Efficient induction of hMSC differentiation and better understanding of hMSCs behaviors in vitro and in vivo are essential to the clinical translation of stem cell therapy. Here a quantum dots (QDs)-based multifunctional nanoparticle (RGD-β-CD-QDs) is developed for effective enhancing differentiation and long-term tracking of hMSCs in vitro and in vivo. The RGD-β-CD-QDs are modified with β-cyclodextrin (β-CD) and Cys-Lys-Lys-Arg-Gly-Asp (CKKRGD) peptide on the surface. The β-CD can harbor hydrophobic osteogenic small molecule dexamethasone (Dex) and the RGD peptide not only facilitates the complexation of siRNA and delivers siRNA into hMSCs but also leads to cellular uptake of nanoparticles by RGD receptor. Co-delivery of Dex and siRNA by RGD-β-CD-QDs nanocarrier significantly expedites and enhances the osteogenesis differentiation of hMSCs in vitro and in vivo by combined effect of small molecule and RNAi. Furthermore, the RGD-β-CD-QDs can be labeled with hMSCs for a long-term tracking (3 weeks) in vivo to observe the behaviors of implanted hMSCs in animal level. These findings demonstrate that the RGD-β-CD-QDs nanocarrier provides a powerful tool to simultaneously enhance differentiation and long-term tracking of hMSCs in vitro and in vivo for regenerative medicine.

1. Introduction

Mesenchymal stem cells (MSCs) have emerged as a clinically relevant cell source for regenerative medicine due to their potential to differentiate into several mesenchymal lineages such as adipocytes, osteoblasts, and chondrocytes.[1] This multipotency of MSCs should be useful in many clinical applications including the regeneration of damaged and injured tissues.[2,3] For example, delayed union, or nonunion, of fractured bone remains one of the major clinical complications in bone surgery despite advances in operative techniques. Stem cell therapy holds great promise to the expedited healing of injured bone. However, inducing the differentiation of MSCs efficiently towards an intended lineage, especially the osteogenic lineage, remains a challenge. Conventional osteogenic differentiation protocols require 3–4 weeks to fully differentiate MSCs into mature osteoblastic phenotypes.[4] Furthermore, the extent of differentiation is generally not homogeneous among different cells, thereby leading to subpopulations of less committed stem cells.[5] To date, a number of small molecules are used to regulate a variety of stem cell behaviors including pluripotency, differentiation, and reprogramming.[6] For example, dexamethasone (Dex) has been shown to promote osteogenesis of stem cells by targeting specific intracellular factors.[7] However, because most of the small molecules are hydrophobic, organic solvents such as dimethyl sulfoxide (DMSO) are often used to dissolve the small molecules for cell culture supplementation, which may cause cytotoxicity and impair the differentiation of the treated stem cells. The poor water solubility also hinders the clinical application of these small molecule drugs. In addition to the small molecules, RNA interference (RNAi) as a powerful technology for sequence-specific suppression of gene expressions has been used to regulate the behavior of stem cells like differentiation and so on.[8–12] But the therapeutic applications of RNAi are still limited mainly due to poor cellular uptake and accelerated degradation of siRNAs in biological fluids, and efficient siRNA delivery remains a bottleneck problem for the extensive application of RNAi therapy.[13] Therefore, there is an

Dr J. Li, Dr J. Xu, K. Zhang, Prof. L. Bian
Department of Mechanical and Automation Engineering
The Chinese University of Hong Kong
Hong Kong
E-mail: lbian@mae.cuhk.edu.hk
Dr W. Y. Lee, T. Wu, Prof. G. Li
Faculty of Medicine
The Chinese University of Hong Kong
Hong Kong
Prof. J. Xia
Department of Chemistry
The Chinese University of Hong Kong
Shatin, Hong Kong SAR, China
Prof. L. Bian
Shenzhen Research Institute
The Chinese University of Hong Kong
Hong Kong
Prof. L. Bian
China Orthopedic Regenerative Medicine Group (CORMed)
Hong Kong, China

DOI: 10.1002/adhm.201500879

urgent need to develop an effective delivery system to realize the full potential of RNAi technology and hydrophobic small molecules for enhancing the differentiation of MSCs, and this delivery system will be crucial to the development of effective stem cell therapies to expedite the bone regeneration in the cases of delayed union or nonunion of fracture.

On the other hand, developing a simple and effective probe to label stem cells is also crucially needed in biological science research for the long-term tracking of proliferation, migration, and differentiation of stem cells in vivo. To further optimize stem cell therapy, it is necessary to discern the relative contribution of the implanted MSCs to the tissue regeneration compared to the host cells. A good understanding of the migration and distribution of the implanted stem cells in vivo is also imperative to improve the efficacy and safety of stem cell therapy. Thus, the long-term labeling of stem cells is essential to achieving a better understanding on the fate, migration, and grafting of the administered stem cells in vivo.[14,15] Therefore, we believe that developing a multifunctional system to deliver siRNA and hydrophobic small molecules for enhancing the differentiation of MSCs and simultaneously monitoring the locations of stem cells after transplantation would be of great significance. For such a model system, quantum dots (QDs) offer great potential with the following advantages: (1) QDs are small in size and have a versatile surface chemistry, thereby allowing further surface conjugation of functional groups in order to facilitate drug loading and cellular uptake; (2) QDs are generally photostable and maintain fluorescent intensity in the cell culture for a prolonged time; (3) more importantly, the use of QDs-based nanocarriers offers superb optical properties for real-time monitoring of the biotransport of the nanocarriers and the associated drug release at both the cellular and systemic levels.[16,17]

In this contribution, we demonstrated the synthesis and application of the multifunctional QDs-based nanocarrier (RGD-β-CD-QDs) for the delivery of osteogenic small molecule Dex and siRNA, simultaneously, to enhance osteogenic differentiation effectively and enable long-term tracking of hMSCs in vitro and in vivo (**Scheme 1**). The CdTe/ZnS core/shell QDs were modified with Cys-Lys-Lys-Arg-Gly-Asp (CKKRGD, Bankpeptide Ltd) peptide and amino-beta-cyclodextrin (NH_2-β-CD, Scheme S1A, Supporting Information) on the surface to yield the RGD-β-CD-QDs nanocarrier. The RGD peptide conjugation of the nanocarrier not only promotes the cell adhesion of nanocarrier for cellular uptake but also can bind and deliver siRNA into hMSCs for enhancing the osteogenic differentiation by RNAi. The hydrophobic cavity of β-CDs conjugates assists the loading of the hydrophobic Dex, thereby improving the water solubility of Dex for avoiding the use of cytotoxic organic solvents in cell culture and enhancing the efficiency of osteogenic differentiation. The delivery of siRNA or Dex by RGD-β-CD-QDs significantly improves the osteogenic differentiation of hMSCs when compared to direct media supplementation of Dex. Co-delivery of siRNA and Dex by RGD-β-CD-QDs further enhances the efficiency of osteogenic differentiation in vitro and in vivo. More importantly, the stable fluorescent signal of RGD-β-CD-QDs nanocarrier enables real-time monitoring of the nanocarrier/drugs cellular uptake in vitro and long-term tracking of hMSCs after implantation in vivo, which will furnish important information for determining the efficacy of stem cell therapy.

2. Results and Discussion

2.1. Synthesis and Characteristics of QDs Nanocarrier

To fabricate the RGD-β-CD-QDs nanocarrier, we chose cadmium telluride (CdTe) QDs as the core because of the high luminescence and narrow particle size distribution.[18] Subsequently, a zinc sulfide (ZnS) shell was added to form the core/shell structure (CdTe/ZnS) and the 3-mercaptopropionic acid (MPA) was used as the stabilizer and sulfur source. Compared to the CdTe QDs, the CdTe/ZnS core/shell QDs have higher photoluminescence intensity, better stability, and improved biocompatibility, and therefore are more suitable for biological applications.[19] The MPA-CdTe/ZnS QDs were then cross-linked with 3-aminophenyl boronic acid to covalently conjugate NH_2-β-CD.[20] Next, the NH_2-β-CD-QDs were conjugated with RGD peptide (CKKRGD) by MAL-$(PEG)_4$-NHS linker (Scheme S1B, Supporting Information) to form the RGD-β-CD-QDs nanocarrier (Scheme 1A). The transmission electron microscope (TEM) analysis result reveals that the obtained RGD-β-CD-QDs nanocarrier has an average diameter of ≈4 nm (**Figure 1**A), and the dynamic light scattering (DLS) analysis of RGD-β-CD-QDs in PBS indicates an average diameter of ≈5 nm (Figure 1B). Compared to the naked QDs (MPA-QDs), the RGD-β-CD-QDs are slightly larger but not significantly different in size as shown by the high magnification TEM images (Figure S1, Supporting Information). It was reported that the QDs generally possess a small core size of <10 nm in diameter, and this renders QDs one of the smallest platforms for engineering drug delivery vehicles.[16] The compact size facilitates the cellular uptake of QDs, and this is important to the intracellular delivery of drugs to the stem cells because the stem cells are known for difficult transfection. Furthermore, the strong fluorescence of QDs is another major advantage for monitoring the intracellular trafficking and biodistribution in biomedical applications.[17] As shown in Figure 1C, the RGD-β-CD-QDs nanocarrier displays strong fluorescent emission under excitation, which is essential to the application in the labeling, real-time imaging, and long-term tracking of the hMSCs in vitro and in vivo. The typical absorption and fluorescence emission of RGD-β-CD-QDs was then analyzed by UV–vis and fluorospectrometer (Figure 1D) and the results indicate that our RGD-β-CD-QDs nanocarrier has broad excitation spectra and narrow emission spectra that make it an ideal choice for labeling living cell in vitro and tracking cells over long term in vivo.[21]

The surface modification of QDs with CDs has been shown to reduce cytotoxicity and enhance biocompatibility.[22] This manipulation not only preserves the imaging capabilities of the nanocarrier but also potentially affords the nanocarrier additional therapeutic functionalities such as drug loading. For instance, the hydrophobic cavity of CDs can enhance the solubility, stability, and bioavailability of the delivered hydrophobic drugs.[23] In this study, the NH_2-β-CD was used to conjugate on the surface of the RGD-β-CD-QDs nanocarrier for loading the hydrophobic Dex, thereby improving the water solution of Dex to eliminate the use of cytotoxic organic solvents such as DMSO in cell culture and enhancing the efficiency of osteogenic induction in hMSCs. Moreover, the conjugation of RGD peptide

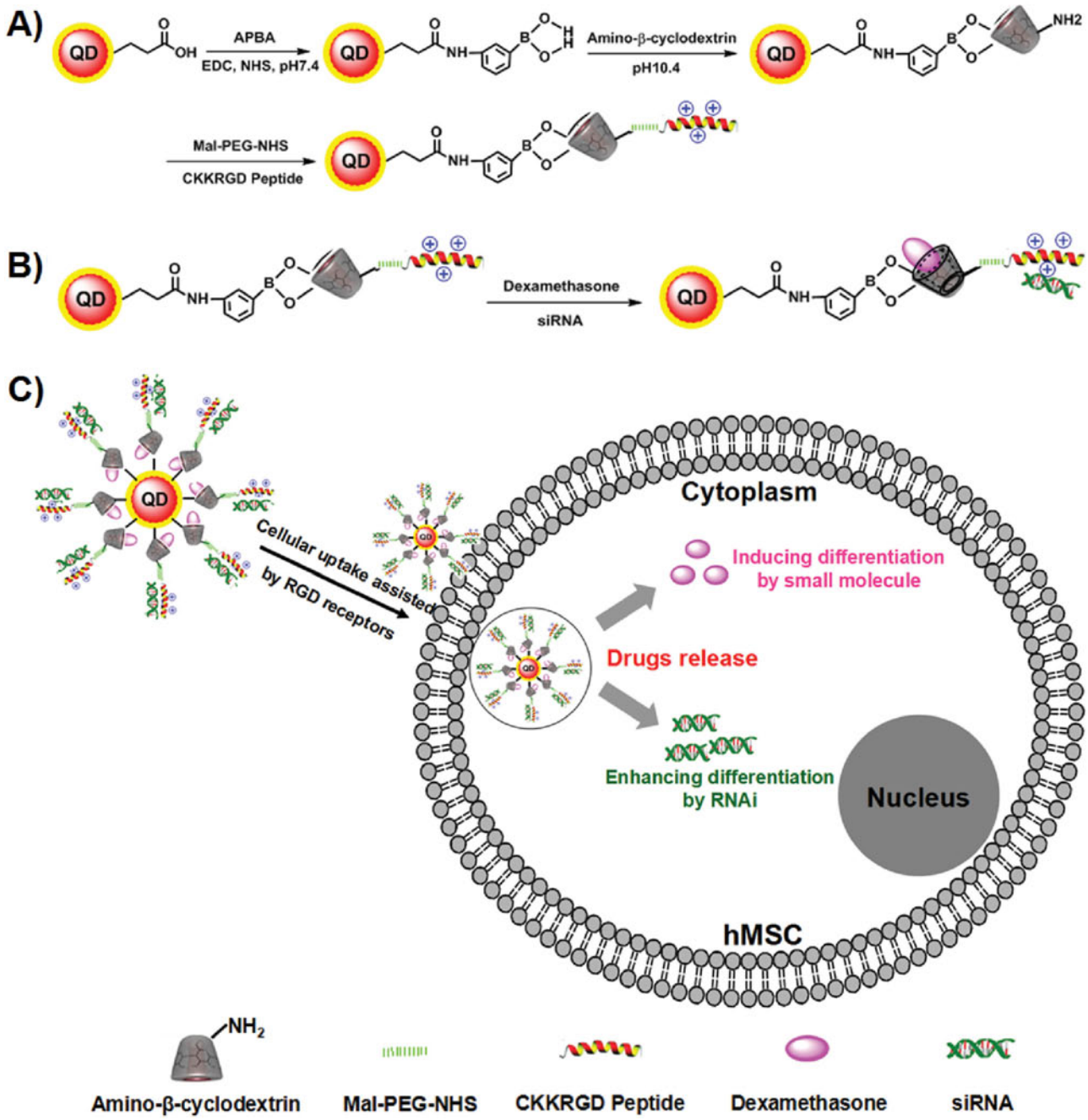

Scheme 1. Synthesis and application of the RGD-β-CD-QDs nanocarrier for enhancing osteogenic differentiation and long-term tracking of hMSCs. A) Synthesis route of the RGD-β-CD-QDs. B) Loading siRNA and Dex onto RGD-β-CD-QDs. C) Co-delivery of Dex and siRNA into hMSCs with RGD-β-CD-QDs for enhancing the osteogenic differentiation of hMSCs and long-term tracking hMSCs by the fluorescence of RGD-β-CD-QDs.

(CKKRGD) with RGD-β-CD-QDs nanocarrier not only provides the positive charge to bind and deliver siRNA into hMSCs for enhancing the osteogenic differentiation by RNAi but also promoting the cell uptake of drugs loaded nanocomplexes by the membranous receptors of cells. After conjugating with β-CD and RGD peptide, the successful synthesis of RGD-β-CD-QDs is confirmed by agarose gel electrophoresis and Fourier transform infrared spectroscopy (FTIR). In Figure 1E, the gel electrophoresis result shows the differing surface charge and motility of MPA-QDs, NH_2-β-CD-QDs, and RGD-β-CD-QDs, thus indicating the successful synthesis of RGD-β-CD-QDs. The FTIR results further show the successful conjugation of β-CD as evidenced by the characteristic symmetric and antisymmetric stretching of C—C from β-CD at 1220 cm^{-1}, and conjugation of RGD peptide as evidenced by the characteristic Amide I band at 1630 cm^{-1} and Amide II band at 1552 cm^{-1} peak (Figure 1F).

Cytotoxicity always is a problem that needs to be considered in the biological applications of QDs as nanocarriers or probes.

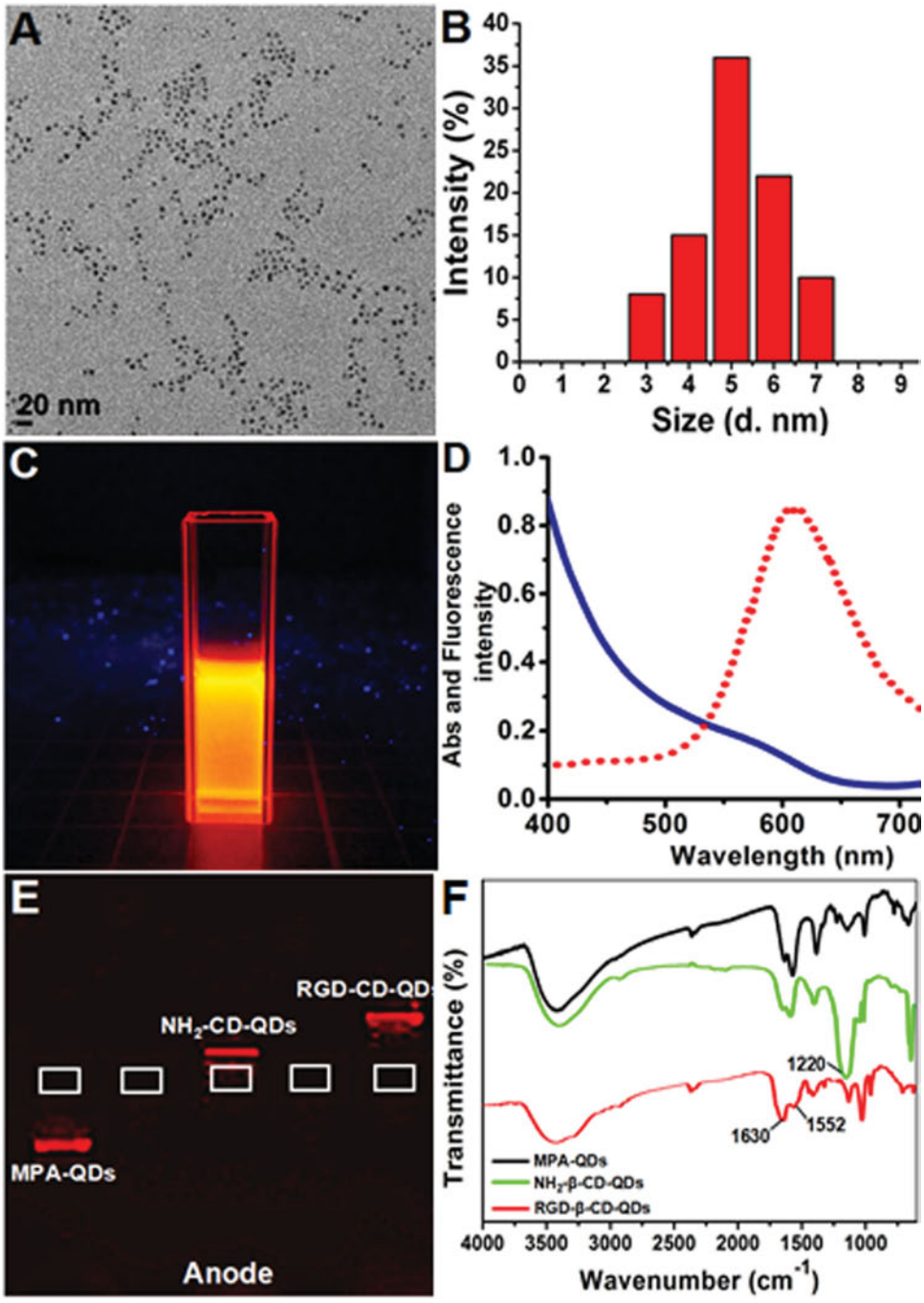

Figure 1. The characterisation of RGD-β-CD-QDs nanocarrier. A) TEM image of the RGD-β-CD-QDs. B) DLS analysis of the RGD-β-CD-QDs. C) Fluorescence emission of the RGD-β-CD-QDs under UV excitation. D) UV absorption and fluorescence spectra of the RGD-β-CD-QDs. E) Agarose gel analysis of the MPA-QDs, NH_2-β-CD-QDs, and RGD-β-CD-QDs. F) FTIR of the MPA-QDs (black), NH_2-β-CD-QDs (green), and RGD-β-CD-QDs (red).

We evaluated the cytotoxicity of RGD-β-CD-QDs nanocarrier by Alamar blue assay (Figure S2, Supporting Information). The cytotoxicity of the nanocarrier is generally low in hMSCs at a concentration up to 200×10^{-9} M after 24 h of incubation. It is worth noting that the conjugation of β-CD improves the hMSCs viability (NH_2-β-CD-QDs >80% viable vs MPA-QDs <80% viable at 200×10^{-9} M). Despite a slight decrease in the hMSCs viability after the RGD peptide conjugation of QDs, the hMSCs viability in the presence of this high dosage of RGD-β-CD-QDs is still over 80%, thus indicating the low overall cytotoxicity of our nanocarrier as a result of the CdTe/ZnS core/shell structure and β-CD modification. Furthermore, the long-term cytotoxicity study with 20×10^{-9} M of the RGD-β-CD-QDs nanocarrier shows minimal cytotoxicity to hMSCs, and the viability of hMSCs is more than 90% after 12 d of incubation (Figure S3, Supporting Information).

2.2. Cell Uptake Study of QDs Nanocarrier

After confirming the cytotoxicity of RGD-β-CD-QDs nanocarrier, we tested whether the nanocarrier can enter hMSCs efficiently for drug delivery and long-term tracking in vitro. As shown in **Figure 2**A, the confocal images indicate that our nanocarrier can enter into hMSCs efficiently and label the proliferating cells for up to 7 d of culture at 20×10^{-9} M concentration. This is consistent with a previous study that reported the optimized effective QDs concentration for labeling MSCs at $\approx 20 \times 10^{-9}$–$50 \times 10^{-9}$ M.[24] On the other hand, the conjugation of RGD peptide with materials is able to promote the adhesion between materials and stem cell,[25,26] thereby promoting the cellular uptake of RGD peptide-conjugated nanoparticles.[27] Thus, compared to the QDs without RGD modification (MPA-QDs, NH_2-β-CD-QDs), the RGD-β-CD-QDs nanocarrier shows more efficient cell uptake of hMSCs by confocal microscopy (Figure S4A, Supporting Information) and flow cytometry (Figure S5, Supporting Information). Furthermore, the RGD-β-CD-QDs nanocarrier shows efficient cell uptake by the hMSCs after 3 h of incubation, and the red fluorescence of the QDs can be observed in the cytoplasm of the hMSCs from the bright field/fluorescence merged images (Figure S4B, Supporting Information).

The subsequent internalization (macropinocytosis) of the bound nanocarrier also results in the localization of the nanocarrier inside the intracellular structures of endosome characteristics after 3 h of incubation (Figure S6, Supporting Information). It was reported that the delivery process of peptide-conjugated QDs starts with the binding of QDs with plasma membranes and filopodia, leading to the internalization of QDs by macropinocytosis. This is followed by active transport of the QDs-containing vesicles from the cell periphery to the intracellular space.[28] In addition, the Bio-TEM images also confirm that the internalized RGD-β-CD-QDs are located in the cytoplasm of the hMSCs after 1 d of incubation and stay in the cytoplasm for up to 7 d (Figure 2B). Meanwhile, the RGD-β-CD-QDs labeling does not affect the osteogenic differentiation of hMSCs as shown by the robust ALP activity after transfection (Figure S7, Supporting Information).

2.3. Delivery of siRNA and Dex by QDs Nanocarrier

We then examined the complexation of siRNA to the RGD-β-CD-QDs nanocarrier. As shown in **Figure 3**A, the gel electrophoresis result indicates that increasing the nanocarrier dosage (from 0 to 20×10^{-9} M) reduces the mobility of the fluorescent $siRNA^{FAM}$ in the gel during electrophoresis, thus demonstrating that

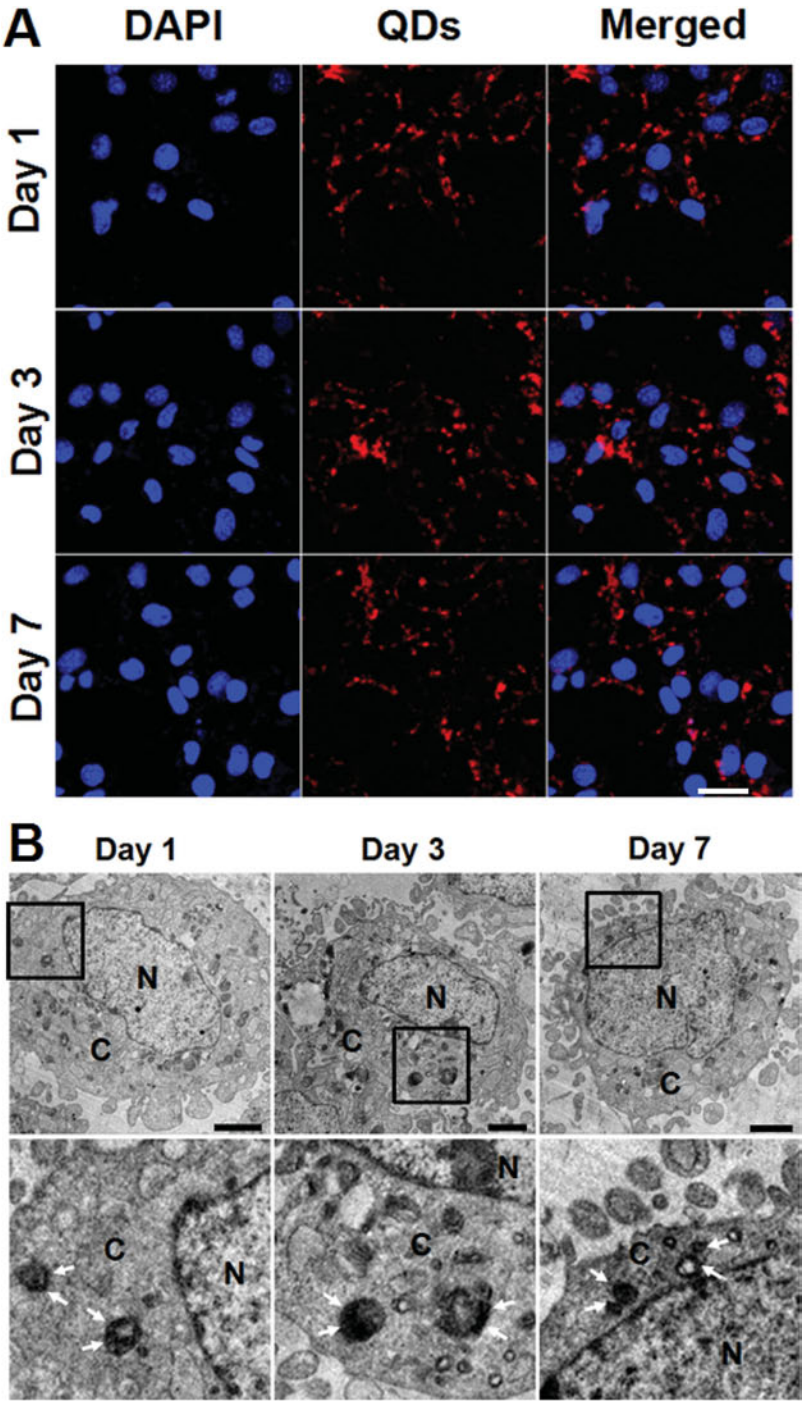

Figure 2. Long-term labeling of hMSCs with RGD-β-CD-QDs nanocarrier. A) Confocal images of the RGD-β-CD-QDs labeled hMSCs after 1, 3, and 7 d of culture. RGD-β-CD-QDs concentration: 20×10^{-9} M; DAPI: Ex 405 nm, Em 435–455 nm; QDs: Ex 405 nm, Em 595–615 nm. Scale bar: 20 μm. B) Bio-TEM images of the RGD-β-CD-QDs labeled hMSCs after 1, 3, and 7 d of culture. The high magnification Bio-TEM images show the aggregation of RGD-β-CD-QDs in the cytoplasm of the hMSCs (white arrows). Scale: 5 μm.

RGD-β-CD-QDs can complex with siRNA efficiently. When the concentration of the nanocarrier is 20×10^{-9} M, the siRNAs^{FAM} (200×10^{-9} M) are completely restricted in the sample loading well, showing the molar ratio between the nanocarrier and siRNA (1:10) is optimal for the following experiments. Furthermore, we studied the delivery kinetics of siRNA by the nanocarrier in hMSCs. In Figure 3B, the confocal images show the time-dependent accumulation of the RGD-β-CD-QDs/siRNA^{FAM} nanocomplexes in hMSCs (red: RGD-β-CD-QDs, green: siRNA^{FAM}). After 1 h of incubation, the nanocomplexes attach to the cell membrane of the hMSCs, and after 3 h, the nanocomplexes enter the hMSCs and accumulate (in the endosome) around the cell nuclei. Compared to the red fluorescence of RGD-β-CD-QDs, the green fluorescence of siRNA^{FAM} becomes more intense and distributed in the intracellular space after 5 h of incubation, thus demonstrating the dissociation and subsequent release of the siRNA from the nanocarrier and endosomes in hMSCs. This result also indicates that our QDs nanocarrier can be used as a powerful probe for the real-time monitoring of cellular behaviors such as transfection and drug release in the stem cells research. To load Dex to the RGD-β-CD-QDs nanocarrier, we mixed Dex and the nanocarrier under stirring in PBS for overnight. In Figure S8 (Supporting Information), the FTIR result reveals that the Dex is loaded into the nanocarrier successfully. Furthermore, the UV–vis analysis indicates that the optimal molar ratio between the nanocarrier and Dex for the most efficient complexation is 1:5, which is used for the following experiments (Figure S9, Supporting Information). After loading Dex at the optimized ratio, the zeta potential and size of the RGD-β-CD-QDs/Dex nanocomplexes differs slightly from that of the RGD-β-CD-QDs nanoparticles, but the zeta potential of the RGD-β-CD-QDs/Dex/siRNA nanocomplexes significantly decreases, indicating the successful complexation of the negatively charged siRNA (Table S1, Supporting Information).

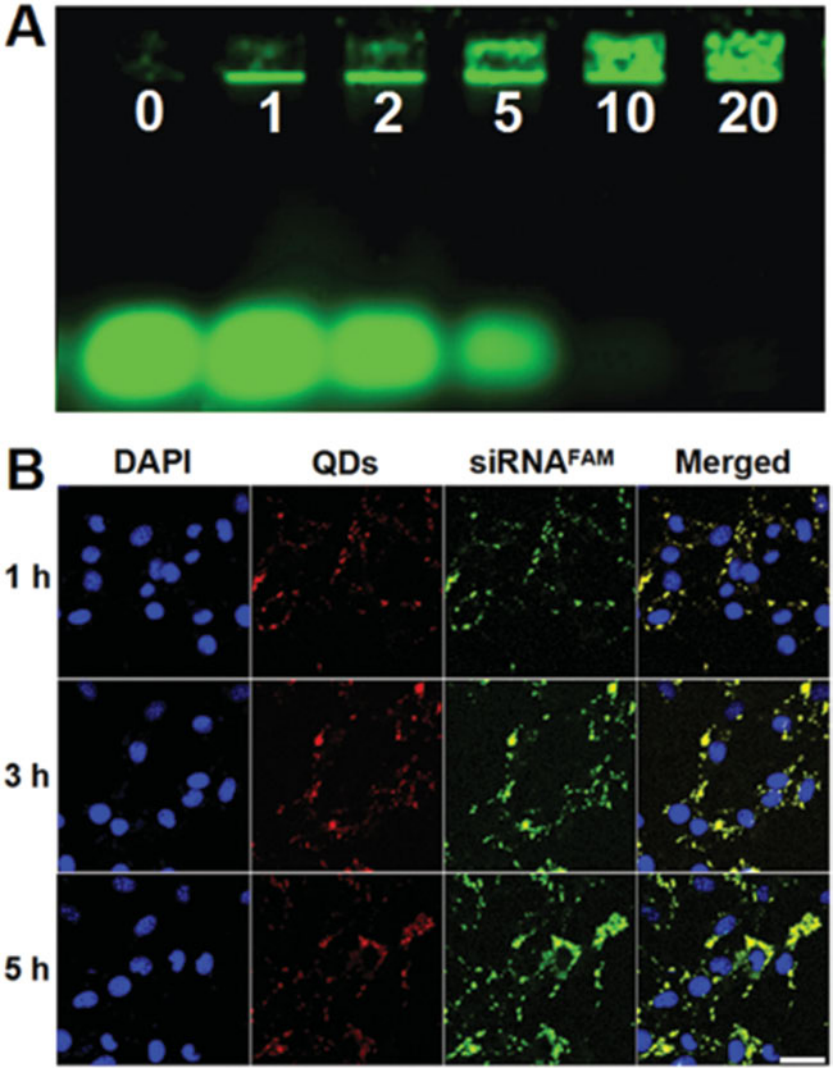

Figure 3. Binding and delivering siRNA into hMSCs by the RGD-β-CD-QDs nanocarrier. A) Effective binding of siRNA onto the RGD-β-CD-QDs as determined by agarose gel electrophoresis. Increasing concentration of RGD-β-CD-QDs (from 1 to 20×10^{-9} M) reduces the mobility of the siRNA^{FAM} during electrophoresis, thus indicating the formation of RGD-β-CD-QDs/siRNA^{FAM} nanocomplexes. B) Real-time monitoring the transfection of the RGD-β-CD-QDs/siRNA^{FAM} nanocomplexes after 1, 3, and 5 h of incubation with hMSCs by confocal. RGD-β-CD-QDs: 20×10^{-9} M; siRNA^{FAM}: 200×10^{-9} M. DAPI: Ex 405 nm, Em 435–455 nm; siRNA^{FAM}: Ex 488 nm, Em 515–535 nm; RGD-β-CD-QDs: Ex 405 nm, Em 595–615 nm. Scale bar: 20 μm.

2.4. Co-delivery of siRNA and Dex by QDs Nanocarrier to Enhance Differentiation

Next, we tested the gene silencing capability of RGD-β-CD-QDs nanocarrier by delivering siRNA against peroxisome proliferator-activated receptor gamma (PPARγ) by reverse transcription polymerase chain reaction (RT-PCR). The PPARγ is a master regulator of the adipogenesis of MSCs, and the down-regulated expression of PPARγ promotes osteogenic differentiation.[29] The RT-PCR result reveals that treatment with the RGD-β-CD-QDs/siPPARγ nanocomplexes have a significantly higher efficiency of silencing the PPARγ expression (Figure S10 (Supporting Information), down by 73% ± 3.3%) compared to a traditional delivery vector (Lipofectamine 2000, down by ≈35%). Interestingly, the RGD-β-CD-QDs/Dex/siPPARγ nanocomplexes also produce high PPARγ silencing efficiency (down by 70% ± 7.2%), thus indicating loading Dex with RGD-β-CD-QDs nanocarrier without compromising the siRNA delivery and gene silencing efficiency. Furthermore, the expression of Runx2 (a major osteogenic marker gene)[30] is also analyzed by RT-PCR and western blot (WB) after

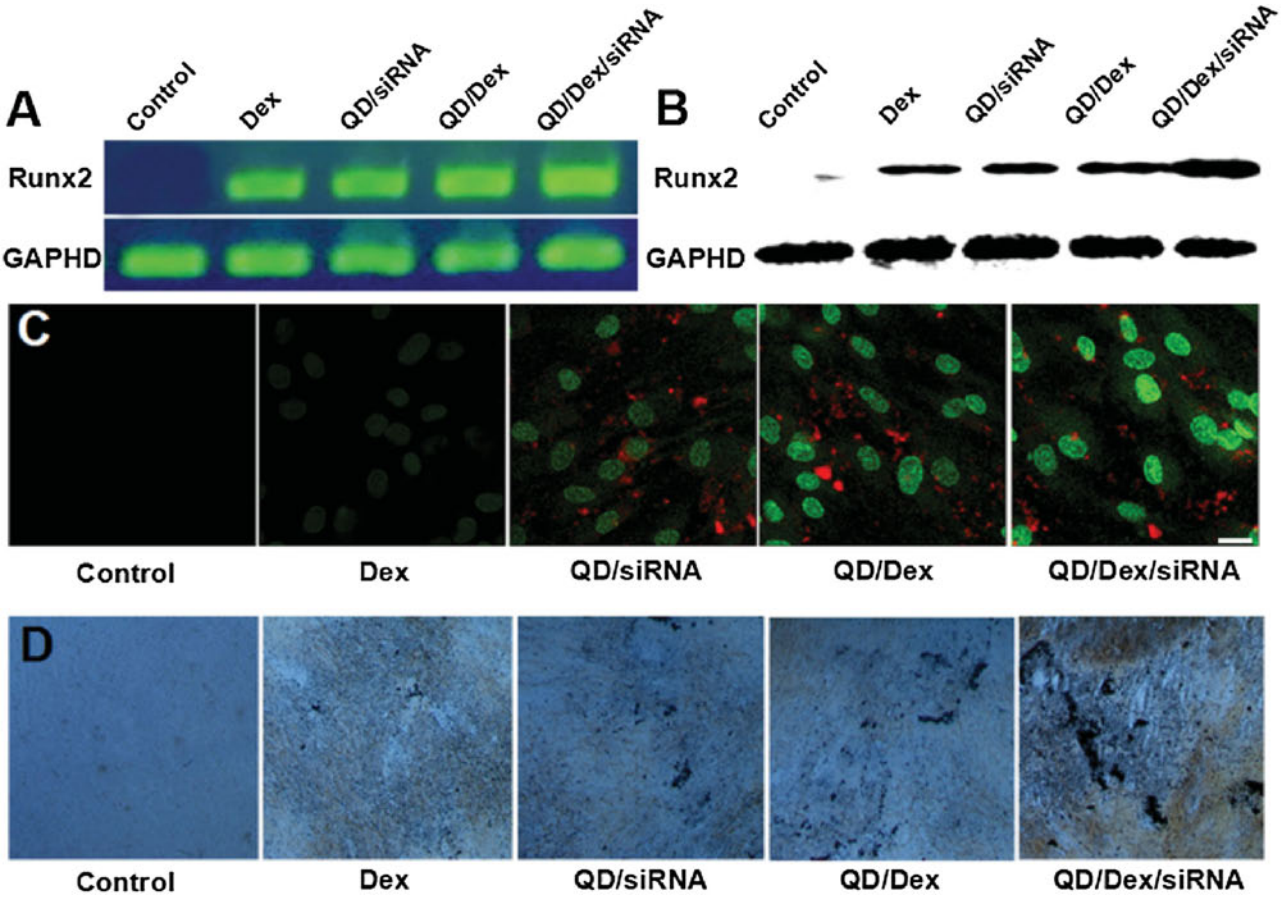

Figure 4. Delivering siRNA and Dex by RGD-β-CD-QDs nanocarrier for enhancing the osteogenic differentiation of hMSCs by promoting the expression of Runx2 with RNAi and small molecule. A) RT-PCR analysis of the Runx2 gene expression in hMSCs after various treatments at day 7. B) Western blot analysis of Runx2 protein expression in hMSCs after various treatments at day 9. C) Confocal images of the immunofluorescence staining against Runx2 (green) in the nucleus of hMSCs after various treatments at day 7. Green: Runx2, Red: RGD-β-CD-QDs, scale bar: 10 μm. D) von Kossa staining of the hMSCs with various treatments at day 12. Magnification: 20×; Control: basal media without Dex, Dex: media supplemented with Dex (100×10^{-9} M), QDs/siRNA: media supplemented with RGD-β-CD-QDs/siRNA nanocomplexes, QDs/Dex: media supplemented with RGD-β-CD-QDs/Dex nanocomplexes, QDs/Dex/siRNA: media supplemented with RGD-β-CD-QDs/Dex/siRNA nanocomplexes. RGD-β-CD-QDs: 20×10^{-9}M; Dex: 100×10^{-9} M; siPPARγ: 200×10^{-9} M.

silencing PPARγ (**Figure 4**A,B). The RT-PCR result indicates that delivering siPPARγ or Dex by RGD-β-CD-QDs enhances the Runx2 expression of the hMSCs substantially (upregulated by 32% ± 5.1% and 57% ± 3.9%, respectively) compared to the positive control (Dex group, osteogenic medium containing 100×10^{-9} M Dex, Runx2 expression: 100% ± 4.2%). Co-delivery of siPPARγ and Dex by RGD-β-CD-QDs results in more than 80% increase in the Runx2 gene expression (upregulated by 88% ± 7.2%), thus demonstrating the high efficacy of the co-delivery in enhancing the osteogenic differentiation of hMSCs. The WB data show the similar trend of the Runx2 protein expression (Figure 4B). The co-delivery of siPPARγ and Dex by RGD-β-CD-QDs increases the Runx2 protein expression by 73% compared to the Dex group. These findings demonstrate that our nanocarriers are capable of delivering siPPARγ and Dex simultaneously, thereby harnessing the osteogenic action of the two ways (RNAi and small molecules) to enhance the osteogenic differentiation of hMSCs efficiently.

To further confirm the osteogenic differentiation of hMSCs, the experiment of immunofluorescence staining against Runx2 protein was performed (Figure 4C). Usually, the expression of Runx2 protein will increase in the nuclei of hMSCs as a key osteogenic transcription factor after osteogenic induction.[26] In Figure 4C, the confocal images show no green fluorescence in the nuclei of hMSCs after 7 d of culture in control group (basal media without Dex), which means no Runx2 expression in the nuclei of hMSCs without osteogenic induction. Relatively, direct media supplementation of Dex group (osteogenic medium, Dex: 100×10^{-9} M) leads to weak green fluorescence in the nuclei of hMSCs, means that there is weak Runx2 expression. In comparison, the delivery of siPPARγ or Dex with RGD-β-CD-QDs nanocarrier to the hMSCs shows the obvious green fluorescence staining against Runx2 in the nuclei of hMSCs, indicating the strong expression of Runx2. Moreover, the co-delivery of siPPARγ and Dex produces the most intense nuclear fluorescent signal against Runx2, showing the highest expression of Runx2 in the nuclei of hMSCs after osteogenic induction by the

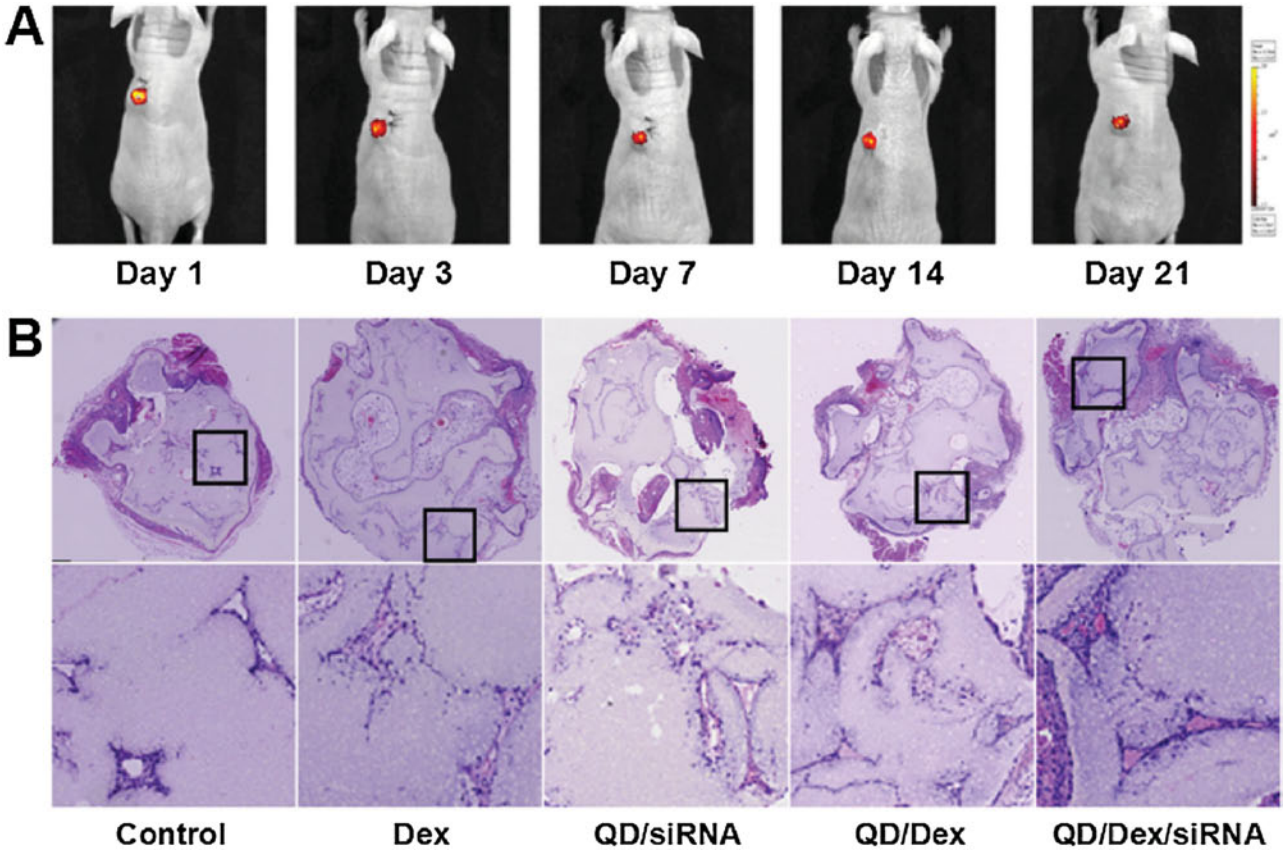

Figure 5. Long-term tracking hMSCs in vivo by labeling RGD-β-CD-QDs with implanted hMSCs and enhancing osteogenic differentiation of hMSCs in vivo by delivering siRNA and Dex with RGD-β-CD-QDs nanocarrier. A) Fluorescent signal of the RGD-β-CD-QDs labeled hMSCs on day 1, 3, 7, 14, and 21 post implantation. B) H&E staining of bone formation by hMSCs with various treatments after 4 weeks of subcutaneous implantation in nude mice. Magnification: 200×.

RGD-β-CD-QDs/Dex/siPPARγ nanocomplexes. In addition, the robust red fluorescence of the QDs nanocarrier detected inside the hMSCs after 7 d of culture demonstrates the capability of our nanocarrier for long term tracking of hMSCs in vitro (Figure 4C). Furthermore, to determine the osteogenic differentiation, hMSCs were cultured with various media treatments and were then stained for mineral deposits by von Kossa staining (Figure 4D) and Alizarin red staining (Figure S11, Supporting Information). The control group (basal media) shows no staining against mineralization, and the Dex group shows weak staining. In comparison, delivering siPPARγ or Dex with our nanocarrier results in substantially more staining against mineralization. The delivery of siPPARγ and Dex simultaneously with our nanocarrier produces the most pronounced mineralization, thus further corroborating the enhanced osteogenic induction by the co-delivery of siPPARγ and Dex with our nanocarrier by the synergistic effect of RNAi and small molecule.

2.5. Long-Term Tracking and Enhancing Diffrentiation of hMSCs In Vivo by QDs Nanocarrier

Finally, to demonstrate the efficacy of RGD-β-CD-QDs nanocarrier for long-term tracking of hMSCs in vivo, we seeded the RGD-β-CD-QDs labeled hMSCs in a porous scaffold and then implanted the scaffold in subcutaneous pockets on the back of nude mice. As shown in **Figure 5**A, the fluorescent signal of the labeled hMSCs can be observed in the back of the nude mice from day 1 to day 21 post implantation, suggesting that the nanocarrier labeling enables long-term tracking of hMSCs in vivo. Furthermore, the fluorescence intensity of the nanocarrier labeled hMSCs is maintained for up to 21 d in vivo with little fluorescent signal reduction (Figure S12, Supporting Information), and this is likely due to the relatively slow exocytosis of nanoparticles from MSCs.[31] This finding demonstrates the potential utility of our nanocarrier as an imaging agent for long-term tracking of stem cells in vivo.

Furthermore, we examined the osteogenic differentiation of hMSCs in vivo after preimplantation culturing in selected media (Figure 5B). 4 weeks after implantation, the hMSC-seeded scaffolds were harvested and prepared for Hematoxylin and eosin (H&E) staining. The H&E staining result shows that delivering siRNA or Dex by RGD-β-CD-QDs to the hMSCs during the preimplantation culture results in more bone tissue deposition in vivo compared to the Dex group as evidenced by the H&E staining (pink staining). The co-delivery of siRNA and Dex by our nanocarrier induces the largest amount of bone tissue deposition, thus further confirming the efficacy of the co-delivery mediated by our nanocarrier in promoting osteogenic differentiation of hMSCs in vivo.

3. Conclusion

In summary, we developed a multifunctional RGD-β-CD-QDs nanocarrier for enhancing osteogenic differentiation and enabling long-term tracking of hMSCs. To the best of our knowledge, this is the first demonstration of inducing stem cell differentiation and tracking implanted stem cells in vivo simultaneously for an extended period with a single multifunctional vehicle. The advantages of our nanocarrier for manipulating stem cell behaviors include: (1) the surface modification of the positively charged RGD peptide aids the efficient cellular uptake and the complexation of siRNA for effective stem cell transfection; (2) the modification of β-CD not only reduces the cytotoxicity and enhances the biocompatibility of RGD-β-CD-QDs but also allows the harboring of hydrophobic small molecules and avoids the use of toxic organic solvents in cell culture; (3) the co-delivery of siRNA and small molecules by a single nanocarrier enhances stem cell differentiation efficiently in vitro and in vivo; (4) the strong fluorescence of RGD-β-CD-QDs can be used as a probe to label stem cells efficiently for long-term tracking in vivo after cell injection and implantation, which will yield valuable information to improve the efficacy and safety of stem cell therapy. While the nanotechnologies in the stem cells research is developing, we believe that our nanocarrier will be instrumental to the development of effective stem cell therapies for expediting the healing of delayed union or nonunion bone fractures.

Supporting Information

Supporting Information is available from the Wiley Online Library or from the author.

Acknowlegement

The work described in this paper was supported by an Early Career Scheme grant from the Research Grants Council of Hong Kong (Project No. 439913). This research is also supported by project BME-p3-15 of the Shun Hing Institute of Advanced Engineering, The Chinese University of Hong Kong. Project 31300796 is supported by the National Natural Science Foundation of China. This research is supported by the Chow Yuk Ho Technology Centre for Innovative Medicine, The Chinese University of Hong Kong. We declare that none of us has any conflict of interest.

Received: November 1, 2015
Revised: December 18, 2015
Published online: February 25, 2016

[1] M. F. Pittenger, A. M. Mackay, S. C. Beck, R. K. Jaiswal, R. Douglas, J. D. Mosca, M. A. Moorman, D. W. Simonetti, S. Craig, D. R. Marshak, *Science* **1999**, *284*, 143.
[2] F. P. Barry, J. M. Murphy, *Int. J. Biochem. Cell Biol.* **2004**, *36*, 568.
[3] S. Wang, X. Qu, R. C. Zhao, *J. Hematol. Oncol.* **2012**, *5*, 19.
[4] K. Flagler, V. Alexeev, E. A. Pierce, O. Igoucheva, *Gene Ther.* **2008**, *15*, 1035.
[5] A. H. Huang, M. J. Farrell, R. L. Mauck, *J. Biomech.* **2010**, *43*, 128.
[6] C. A. Lyssiotis, L. L. Lairson, A. E. Boitano, H. Wurdak, S. Zhu, P. G. Schultz, *Angew. Chem. Int. Ed.* **2011**, *50*, 200.
[7] N. Jaiswal, S. E. Haynesworth, A. I. Caplan, S. P. Bruder, *J. Cell Biochem.* **1997**, *64*, 295.
[8] M. O. Andersen, D. Q. S. Le, M. W. Chen, J. V. Nygaard, M. Kassem, C. Bunger, J. Kjems, *Adv. Funct. Mater.* **2013**, *23*, 5599.
[9] D. M. Fan, E. De Rosa, M. B. Murphy, Y. Peng, C. A. Smid, C. Chiappini, X. W. Liu, P. Simmons, B. K. Weiner, M. Ferrari, E. Tasciotti, *Adv. Funct. Mater.* **2012**, *22*, 282.
[10] B. Shah, P. T. Yin, S. Ghoshal, K. B. Lee, *Angew. Chem. Int. Ed.* **2013**, *52*, 6190.
[11] X. T. Shi, S. Chen, J. H. Zhou, H. J. Yu, L. Li, H. K. Wu, *Adv. Funct. Mater.* **2012**, *22*, 3799.
[12] W. W. Yau, P. O. Rujitanaroj, L. Lam, S. Y. Chew, *Biomaterials* **2012**, *33*, 2608.
[13] H. Siomi, M. C. Siomi, *Nature* **2009**, *457*, 396.
[14] R. Guzman, N. Uchida, T. M. Bliss, D. He, K. K. Christopherson, D. Stellwagen, A. Capela, J. Greve, R. C. Malenka, M. E. Moseley, T. D. Palmer, G. K. Steinberg, *Proc. Natl. Acad. Sci. USA* **2007**, *104*, 10211.
[15] A. B. Rosen, D. J. Kelly, A. J. Schuldt, J. Lu, I. A. Potapova, S. V. Doronin, K. J. Robichaud, R. B. Robinson, M. R. Rosen, P. R. Brink, G. R. Gaudette, I. S. Cohen, *Stem Cells* **2007**, *25*, 2128.
[16] C. E. Probst, P. Zrazhevskiy, V. Bagalkot, X. Gao, *Adv. Drug Deliv. Rev.* **2013**, *65*, 703.
[17] P. Zrazhevskiy, M. Sena, X. Gao, *Chem. Soc. Rev.* **2010**, *39*, 4326.
[18] Y. H. Yang, M. Y. Gao, *Adv. Mater.* **2005**, *17*, 2354.
[19] L. H. Jing, K. Ding, S. Kalytchuk, Y. Wang, R. R. Qiao, S. V. Kershaw, A. L. Rogach, M. Y. Gao, *J. Phys. Chem. C* **2013**, *117*, 18752.
[20] X. Ai, L. Niu, Y. Li, F. Yang, X. Su, *Talanta* **2012**, *99*, 409.
[21] I. L. Medintz, H. T. Uyeda, E. R. Goldman, H. Mattoussi, *Nat. Mater.* **2005**, *4*, 435.
[22] M. X. Zhao, Q. Xia, X. D. Feng, X. H. Zhu, Z. W. Mao, L. N. Ji, K. Wang, *Biomaterials* **2010**, *31*, 4401.
[23] R. Challa, A. Ahuja, J. Ali, R. K. Khar, *AAPS PharmSciTech.* **2005**, *6*, E329.
[24] B. S. Shah, P. A. Clark, E. K. Moioli, M. A. Stroscio, J. J. Mao, *Nano Lett.* **2007**, *7*, 3071.
[25] J. S. Park, H. N. Yang, S. Y. Jeon, D. G. Woo, K. Na, K. H. Park, *Biomaterials* **2010**, *31*, 6239.
[26] X. Wang, C. Yan, K. Ye, Y. He, Z. Li, J. Ding, *Biomaterials* **2013**, *34*, 2865.
[27] C. W. Lu, Y. Hung, J. K. Hsiao, M. Yao, T. H. Chung, Y. S. Lin, S. H. Wu, S. C. Hsu, H. M. Liu, C. Y. Mou, C. S. Yang, D. M. Huang, Y. C. Chen, *Nano Lett.* **2007**, *7*, 149.
[28] G. Ruan, A. Agrawal, A. I. Marcus, S. Nie, *J. Am. Chem. Soc.* **2007**, *129*, 14759.
[29] M. J. Lee, H. T. Chen, M. L. Ho, C. H. Chen, S. C. Chuang, S. C. Huang, Y. C. Fu, G. J. Wang, L. Kang, J. K. Chang, *J. Cell Mol. Med.* **2013**, *17*, 1188.
[30] T. M. Schroeder, E. D. Jensen, J. J. Westendorf, *Birth Defects Res. C Embryo Today* **2005**, *75*, 213.
[31] C. Y. Fang, V. Vaijayanthimala, C. A. Cheng, S. H. Yeh, C. F. Chang, C. L. Li, H. C. Chang, *Small* **2011**, *7*, 3363.

